15. Semlitsch, R. D., Hotz, H. & Guex, G. D. Competition among tadpoles of coexisting hemiclones of hybridogenetic *Rana esculenta*: support for the frozen niche variation model. *Evolution* **51,** 1249–1261 (1997).
16. Weeks, A. R. & Hoffmann, A. A. Intense selection of mite clones in a heterogeneous environment. *Evolution* **52,** 1325–1333 (1998).
17. Jokela, J., Lively, C. M., Fox, J. A. & Dybdahl, M. F. Flat reaction norms and "frozen" phenotypic variation in clonal snails (*Potamopyrgus antipodarum*). *Evolution* **51,** 1120–1129 (1997).
18. Vjijenhoek, R. C. & Pfeiler, E. Differential survival of sexual and asexual *Poeciliopsis* during environmental stress. *Evolution* **51,** 1593–1600 (1997).
19. Case, T. J. Patterns of coexistence in sexual and asexual species of *Cnemidophorus* lizards. *Oecologia* **83,** 220–227 (1990).
20. Doebeli, M. An explicit genetic model for ecological character displacement. *Ecology* **77,** 510–520 (1996).
21. Skelton, P. (ed.) *Evolution: a Biological and Palaeontological Approach* (Addison-Wesley, Wokingham, UK, 1993).
22. Bulmer, M. *Theoretical Evolutionary Ecology* (Sinauer, Sunderland, Massachusetts, 1994).
23. Futuyma, D. J. *Evolutionary Biology* 3rd edn (Sinauer, Sunderland, Massachusetts, 1998).
24. Maynard Smith, J. *Evolutionary Genetics* 2nd edn (Oxford Univ. Press, Oxford, 1998).
25. Stearns, S. C. & Hoekstra, R. F. *Evolution: an Introduction* (Oxford Univ. Press, Oxford, 2000).
26. Case, T. J. & Taper, M. L. On the coexistence and coevolution of asexual and sexual competitors. *Evolution* **40,** 366–387 (1986).
27. Levins, R. in *Lectures on Mathematics in the Life Sciences, vol. 2* (ed. Gerstenhaber, M.) 75–107 (American Mathematical Society, Providence, 1970).
28. Connolly, S. R. & Roughgarden, J. Theory of marine communities: competition, predation, and recruitment-dependent interaction strength. *Ecol. Monogr.* **69,** 277–296 (1999).
29. Lively, C. M. Host-parasite coevolution and sex. *BioScience* **46,** 107–114 (1996).

**Acknowledgements**

We thank G. F. Turner, S. J. Hawkins and C. P. Please for clarifications of key issues. This work was supported by a Natural Environment Research Council grant to C.P.D., and by an Engineering and Physical Sciences Research Council studentship to G.E.P.

Correspondence should be addressed to C.P.D. (e-mail: cpd@soton.ac.uk).

# NMDA spikes in basal dendrites of cortical pyramidal neurons

**Jackie Schiller*, Guy Major†‡, Helmut J. Koester‡§ & Yitzhak Schiller‡‖**

* *Departments of Physiology and Biophysics, Technion Medical School, Bat-Galim, Haifa 31096, Israel*
† *Biological Computation Research-Bell Laboratories, Lucent Technologies, 600 Mountain Avenue, Murray Hill, New Jersey, USA and University Laboratory of Physiology, Oxford, UK*
§ *Department of Cell Physiology, Max-Planck-Institute for Medical Research, Heidelberg, Germany*
‖ *Department of Neurology, Rambam Medical Center, Haifa, Israel*
‡ *These authors contributed equally to this work*

**Basal dendrites are a major target for synaptic inputs innervating cortical pyramidal neurons[1]. At present little is known about signal processing in these fine dendrites. Here we show that co-activation of clustered neighbouring basal inputs initiated local dendritic spikes, which resulted in a 5.9 ± 1.5 mV (peak) and 64.4 ± 19.8 ms (half-width) cable-filtered voltage change at the soma that amplified the somatic voltage response by 226 ± 46%. These spikes were accompanied by large calcium transients restricted to the activated dendritic segment. In contrast to conventional sodium or calcium spikes, these spikes were mediated mostly by NMDA (*N*-methyl-D-aspartate) receptor channels, which contributed at least 80% of the total charge. The ionic mechanism of these NMDA spikes may allow 'dynamic spike-initiation zones', set by the spatial distribution of glutamate pre-bound to NMDA receptors, which in turn would depend on recent and ongoing activity in the cortical network. In addition, NMDA spikes may serve as a powerful mechanism for modification of the cortical network by inducing long-term strengthening of co-activated neighbouring inputs.**

To explore synaptic processing in basal dendrites we identified fine dendritic branches using fluorescence confocal microscopy and mimicked excitatory postsynaptic potentials (EPSPs) by ultraviolet laser glutamate uncaging. Figure 1a compares a synaptically evoked EPSP with an excitatory postsynaptic-like potential (EPSLP) evoked by a 1-ms ultraviolet laser pulse directed to a basal dendrite in the presence of 1 mM extracellular caged glutamate. The two post-synaptic potentials were similar except that EPSLPs were slower and had a larger NMDA component (see Methods for details).

Figure 1b shows EPSLPs evoked in a distal basal dendrite at various laser intensities. At a certain threshold intensity, a small increase in the laser intensity more than doubled the EPSLP amplitude recorded at the soma (Fig. 1b). Beyond that threshold intensity only a small additional increase in EPSLP peak amplitude occurred when the laser power was increased (Fig. 1b, $n = 14$ cells). The threshold and all-or-none nature of the response indicated initiation of local dendritic spikes. The mean amplitude of just subthreshold cable-filtered responses was 3.9 ± 1.1 mV, and the amplitude of the cable-filtered basal dendritic spike was 5.2 ± 1.7 mV, as measured at the soma ($n = 14$). Unless otherwise specified, the terms 'suprathreshold' and 'subthreshold' are taken to mean 'suprathreshold in the dendrite' and 'subthreshold in the dendrite', respectively. All EPSLPs presented were subthreshold with respect to axonal action potentials. Hyperpolarization of the membrane potential reduced the amplitudes of the suprathreshold EPSLPs to subthreshold levels (Fig. 1c, $n = 4$). Calcium imaging revealed that suprathreshold EPSLPs evoked a large localized increase in calcium influx limited to a roughly 20-μm stretch of the activated basal dendrite (Fig. 1d, $n = 5$). These observations are consistent with initiation of a local spike by focal glutamate uncaging onto a single basal dendrite.

Subthreshold EPSLPs were not affected by addition of either the specific voltage-gated sodium channel (VGSC) blocker tetrodotoxin (TTX; 1 μM) (96 ± 10% of control value, $n = 7$) or the voltage-gated calcium channel (VGCC) blocker cadmium (50–150 μM) (95 ± 6% of control value, $n = 10$). In contrast, TTX and cadmium substantially reduced the amplitudes and time integrals of supra-threshold EPSLPs (Fig. 2a, b). The average threshold for basal dendritic spike initiation measured at the soma was 4.2 ± 1.4 mV ($n = 7$) for TTX and 4.4 ± 1.8 mV ($n = 10$) for cadmium. The sodium and calcium-dependent cable-filtered spikes added 5.0 ± 2.1 mV (half-width of 60 ± 16 ms) and 4.7 ± 1.8 mV (half-width of 58 ± 15 ms) to the somatic potential, respectively.

Basal dendritic spikes could be reinitiated following blockade of either VGSCs or VGCCs. The threshold laser intensity for spike initiation increased by 29 ± 6% in the presence of TTX and 101 ± 9% in the presence of cadmium. The reinitiated spikes were similar to the original spikes evoked under control conditions (Fig. 2c). The averaged peak and time integral of the reinitiated spikes were 95.7 ± 8.2% and 117.3 ± 33.5% of the original spikes ($n = 6$). These results indicated that although VGCCs and VGSCs participated in the initiation of the basal dendritic spike, a third dendritic conductance probably served as the major charge carrier. Furthermore, the fact that basal dendritic spikes could be reinitiated in the presence of either TTX or cadmium ruled out the possibility that these spikes resulted from a polysynaptic or circuit effect.

When glutamate was uncaged at the soma, there were no sudden jumps in response amplitude as laser intensity was increased. Furthermore, TTX and cadmium did not noticeably change somatic EPSLPs (101 ± 11% and 104 ± 4% of control, $n = 6$ and 7, respectively). Thus, somatic VGSCs and VGCCs did not contribute to basal dendritic spikes.

Initiation of local basal dendritic spikes was limited to distal basal dendrites (>70 μm away from the soma). In three neurons the difference between the distal and proximal dendrite was observed for the same basal dendrite.

Basal dendritic spikes were critically dependent on activation of


© 2000 Macmillan Magazines Ltd

NMDA receptors. Figure 3a shows that the addition of the NMDA receptor blocker AP5 (D(−)-2-amino-5-phosphonovaleric acid; 100 μM) eliminated the basal dendritic spike evoked under control conditions ($n$ = 12). Increasing the laser intensity further (up to 775% of the control threshold intensity) did not restore the spike. This was true even when we used high-frequency (40–200 Hz) glutamate uncaging ($n$ = 5). In the presence of AP5, the peak and half-width of the AMPA (α-amino-3-hydroxy-5-methyl-4-isoxazolepropionate) receptor-mediated EPSLPs were not changed significantly by the addition of cadmium or TTX (97.8 ± 5.7% and 105.6 ± 5.5% of control values, respectively). More importantly, local basal dendritic spikes were initiated even after we blocked both VGSC and VGCC with TTX and cadmium (Fig. 3b). These spikes in turn were blocked by AP5 (Fig. 3c, $n$ = 5). 'Pure NMDA spikes' in the presence of TTX and cadmium were higher and wider than the spikes recorded under control conditions (peak amplitude of cable-filtered spikes measured at soma was 7.2 ± 2.6 mV, half-width of 77.3 ± 12.7 ms, $P < 0.01$ compared with control spikes). Our findings indicate that local basal dendritic spikes are mediated for the most part by current flowing through NMDA receptor channels. Sodium and calcium channels assist in spike initiation, but are not necessary for it.

We used computer simulations to quantify the relative contributions of NMDA channels, VGSCs and VGCCs to local basal dendritic spikes (Fig. 3d). With the parameters adjusted so that the model matched the experimental observations, the simulations revealed that NMDA receptor channels contributed around 80% of the charge mediating basal dendritic spikes, with sodium and calcium channels together contributing around 20%. Increasing the density of VGSCs and/or VGCCs so that they contributed more than 20% of the current mediating basal dendritic spikes was inconsistent with the experimental findings that AMPA-mediated EPSLPs were unaffected by cadmium and TTX. The experimental finding that the pure NMDA spike was larger than the control spike was consistent with modelling results showing that initiation of pure NMDA spikes required more NMDA conductance. In addition, the simulations revealed that NMDA spikes involved a 'spike-chain' mechanism: the AMPA response evoked a fast local sodium 'spikelet', which elicited a slower calcium-mediated regenerative response, which in turn initiated the full-blown NMDA spike (Fig. 3d).

To investigate whether local basal dendritic spikes can be evoked by synaptic inputs, we combined focal stimulation of basal dendrites with two-photon imaging. As in the uncaging experiments, when we gradually increased the synaptic stimulus intensity there was an abrupt jump in the EPSP amplitude, and a spike-like response was initiated (Fig. 4a, b). The spike initiation was sensitive to the frequency of activation. Although spikes could be observed with a single EPSP ($n$ = 6), they were easier to elicit with high-frequency stimulation (two stimuli at 50–100 Hz; 9 out of 11 neurons examined). At dendritic threshold, the cable-filtered EPSP peak was 2.6 ± 0.8 mV and the cable-filtered basal dendritic spike added 5.9 ± 1.5 mV (226 ± 46%, half-width 64.4 ± 19.8 ms) to the somatic voltage response ($n$ = 6).

The NMDA receptor blocker AP5 (100 μM) selectively reduced the amplitude of EPSPs that crossed the local dendritic threshold and abolished the spike response (Fig. 4b). Furthermore, AP5 linearized the relationship between the synaptic stimulus intensity and EPSP amplitude and eliminated the abrupt jump observed under control conditions (Fig. 4b, $n$ = 4). Basal dendritic spikes could not be reinitiated in the presence of AP5, even with stimulation intensities sufficient to evoke AMPA-mediated EPSPs that were two to three times larger than the just subthreshold EPSPs in control conditions. In control solution sufficient hyperpolarization of the

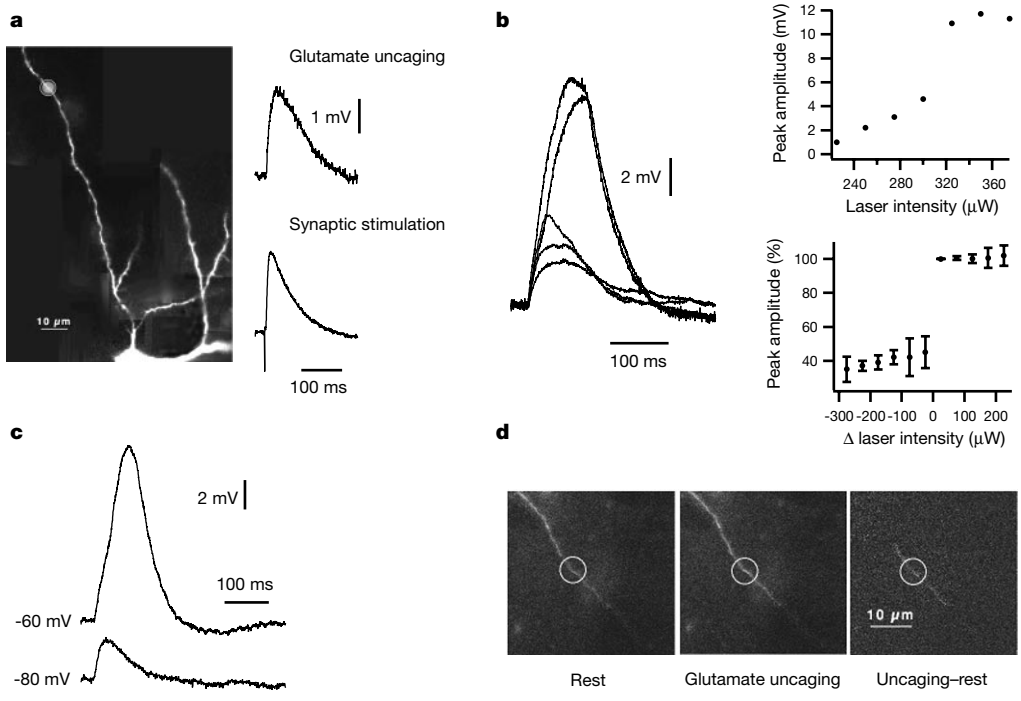


**Figure 1** Local spikes in basal dendrites evoked by focal glutamate uncaging. **a**, Fluorescent image of the basal dendritic arborization (left). The grey spot obtained by flash photolysis of caged fluorescein dextran represents the area of glutamate uncaging. Right, somatic voltage responses evoked by glutamate uncaging at a basal dendrite 150 μm away from the soma (top) and focal synaptic stimulation (bottom) in the same neuron. **b**, Traces of single EPSLPs evoked at increasing laser intensities (left). The peak EPSLP amplitude is plotted as a function of the laser intensity for the cell shown (top right) and for an average of 14 cells (bottom right). The laser intensity is shown relative to the laser intensity at threshold (0). The EPSLP amplitude is presented in per cent of just suprathreshold EPSLP (defined as 100%). **c**, The effect of hyperpolarization of the membrane potential on suprathreshold EPSLP recorded at the soma. **d**, Images of a basal dendritic branch (140 μm from the soma) at rest and during dendritic spike response. The third image represents the net calcium increase during spike initiation. The circle represents the site of the glutamate uncaging.


© 2000 Macmillan Magazines Ltd

membrane potential prevented the dendritic spike response (Fig. 4c, $n = 5$). Together, the last two observations showed that local postsynaptic conductances were responsible for the sharp threshold behaviour, and not recruitment of presynaptic axons or boutons, or polysynaptic circuits.

The similarity between uncaging and synaptically evoked dendritic spikes with respect to amplitude ($P = 0.19$) and half-width ($P = 0.29$), and the fact that synaptically evoked basal dendritic spikes could not be reinitiated in the presence of AP5, indicated that synaptically evoked basal dendritic spikes most probably represent local NMDA spikes. To investigate this further, we performed additional experiments using the intracellular blocker D-890, a predominantly L-type VGCC blocker (Fig. 5a). Initiation of basal dendritic spikes remained intact (peak 5.6 ± 1.14 mV, threshold 2.36 ± 0.38 mV, $n = 4$) in the presence of high concentrations of D-890 (2 mM), despite the fact it reduced the peak of action potential-evoked calcium transients at basal dendrites by 88 ± 8% ($n = 4$). These findings indicated further that synaptically evoked basal dendritic spikes represent NMDA rather than calcium spikes.

Simultaneous two-photon calcium imaging from the spines and shafts of the activated site revealed that basal dendritic NMDA spikes were accompanied by a large rise in intradendritic calcium (Fig. 5b). The peak calcium transient versus stimulus intensity curve showed a threshold behaviour with the same threshold value as was found for the voltage responses (compare Figs 4b and 5b). Addition of AP5 significantly reduced the peak calcium transients (by 92 ± 3% at threshold intensity). Furthermore, as with the voltage responses, AP5 abolished the threshold behaviour, linearizing the intensity response curve (Fig. 5b, $n = 3$). Calcium transients evoked by basal dendritic spikes were restricted to a small segment of a single basal branch (10–20 μm), similar to those described for the

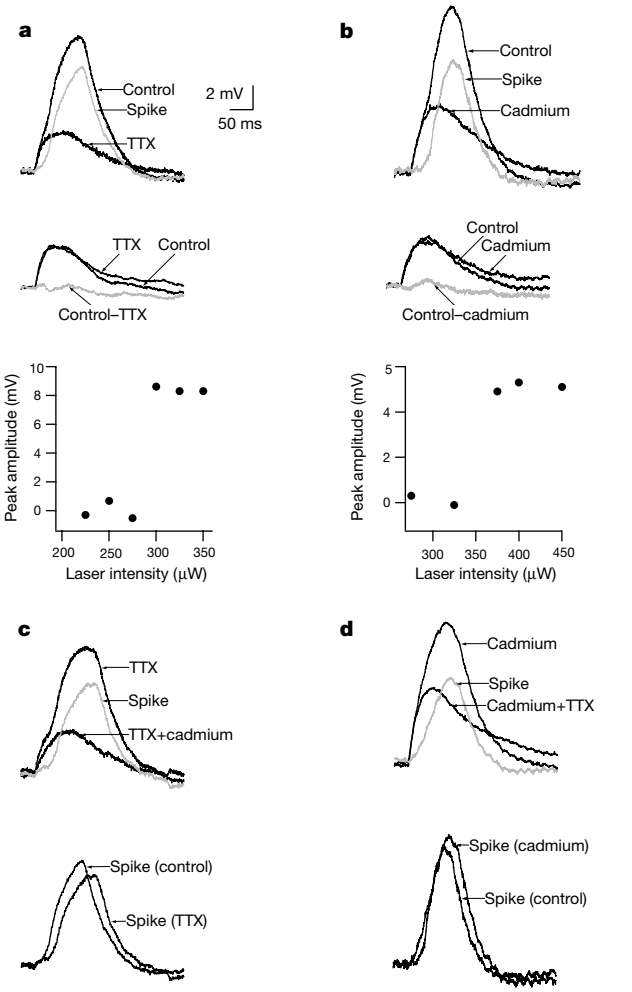


**Figure 2** Voltage-gated sodium and calcium channels participate in initiation of basal dendritic spikes. **a**, **b**, Local subthreshold and suprathreshold EPSLPs before (control) and after extracellular application of TTX (1 μM, **a**) and cadmium (100 μM, **b**). The grey traces (control–TTX, control–cadmium, spike) represent a subtraction of traces with the blockers from control traces. Lower panel: the peak of the net sodium- (left, control–TTX) and calcium-dependent (right, control–cadmium) components are plotted as a function of the laser intensities. **c**, **d**, Reinitiation of spikes in the presence of TTX (1 μM, **c**) and cadmium (100 μM, **d**) upon increasing the laser intensity (29% and 94%, respectively). The reinitiated spikes were blocked in turn by cadmium and TTX, respectively. The traces were obtained from the neurons shown in **a** and **b**, respectively. Lower two traces: The spikes recorded under control conditions are presented for comparison together with the reinitiated spike in the presence of TTX (left) and cadmium (right).

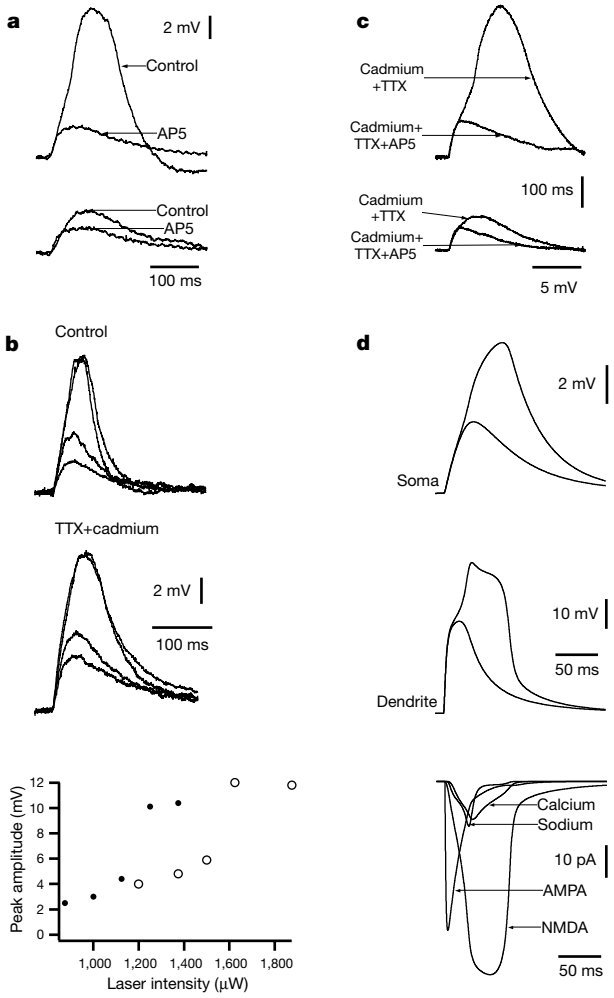


**Figure 3** NMDA receptor channels are the main charge carriers mediating basal dendritic spikes. **a**, Subthreshold (lower traces) and suprathreshold (upper traces) EPSLPs evoked under control conditions and after addition of 100 μM AP5. **b**, Traces of EPSLPs evoked at increasing laser intensities in control conditions and after adding both TTX (1 μM) and cadmium (100 μM, top). Lower panel: peak EPSLP amplitudes are plotted as a function of the laser intensity in control conditions (filled circles) and in the presence of the blockers (empty circles). **c**, 'Pure' NMDA spike evoked by glutamate uncaging in the presence of TTX (1 μM) and cadmium (100 μM) before and after the addition of AP5 (100 μM). **d**, Computer simulations of somatic voltage (top), dendritic voltage (middle) and the corresponding dendritic currents (bottom) are given for just subthreshold and just suprathreshold responses. The currents are shown only for the suprathreshold response. The maximum NMDA (nS), sodium and calcium (mS $cm^{-2}$) conductance densities are $G_{NMDA}$ 11; $G_{Na}$ 2, $G_{CaH}$ 0.02, $G_{CaT}$ 0.15.


© 2000 Macmillan Magazines Ltd

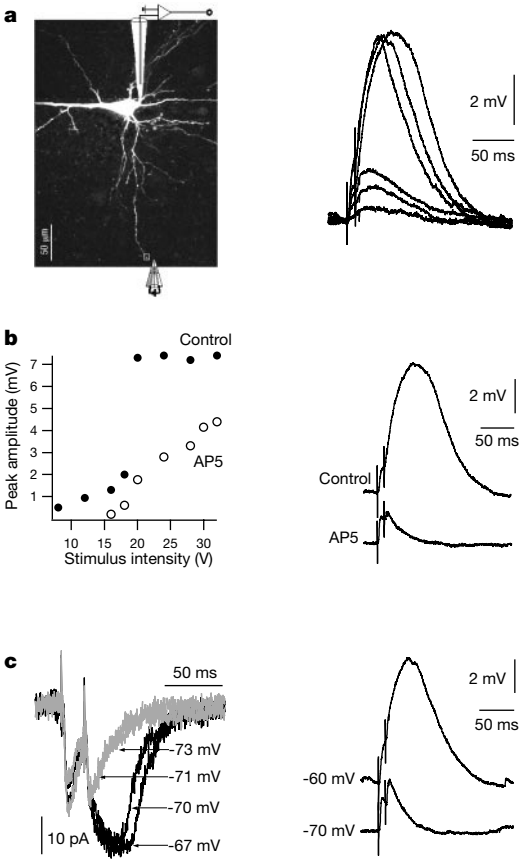


**Figure 4** Basal dendritic NMDA spikes evoked by focal synaptic stimulation. **a**, Fluorescent image of the basal dendritic arborization. A bipolar theta synaptic stimulating electrode (shown schematically) was placed close to a distal basal dendrite (left). Right, postsynaptic voltage responses (two stimuli at 100 Hz) at different stimulus intensities. **b**, The peaks of postsynaptic voltage responses are plotted as a function of synaptic stimulus intensities under control conditions (filled circles) and in the presence of AP5 (100 μM, open circles) (left). Basal dendritic spike in control conditions and after addition of AP5 (100 μM, right). **c**, Synaptically evoked postsynaptic current (voltage-clamp, left) and voltage (current-clamp, right) responses obtained at different hyperpolarizing holding membrane potentials at a single synaptic stimulus intensity that was suprathreshold for spike initiation at the resting membrane potential.

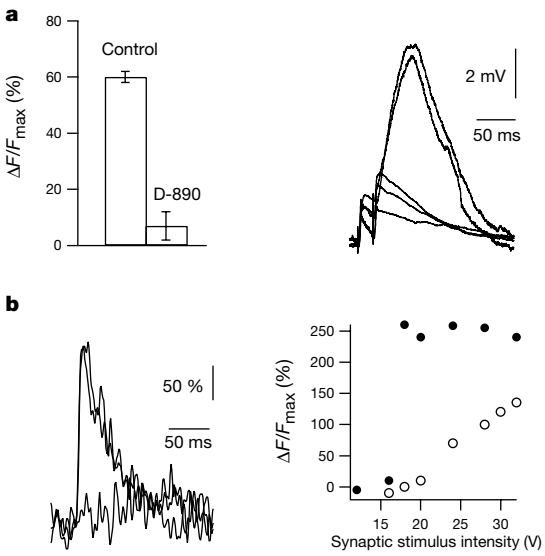


**Figure 5** Synaptically evoked basal dendritic spikes are accompanied by large local calcium influx. **a**, Left, averaged peak dendritic calcium transients (presented as $\Delta F/F$ in per cent) evoked by somatic action potentials in control conditions and in the presence of D-890 (2 mM) in the pipette solution. Right, postsynaptic voltage responses and dendritic spike initiation evoked by focal basal synaptic stimulation (50 Hz) at different stimulus intensities in the presence of D-890 (2 mM). **b**, Calcium transients obtained from an activated dendritic spine during focal synaptic stimulation at different intensities (left). The corresponding voltage traces are shown in Fig. 4a. Right, the peak calcium transients are presented as a function of the stimulus intensity under control conditions (filled circles) and in the presence of AP5 (open circles).

glutamate uncaging experiments. Furthermore, we observed no evidence for activation of neighbouring branches ($n = 3$).

Linear summation of EPSPs within the dendritic trees of CA1 pyramidal neurons has been reported[2,3]. Although NMDA receptor channels did participate in actively linearizing the summation process, basal dendritic NMDA spikes were not reported. This difference could reflect differences between CA1 and layer 5 cortical neurons, or it could be because, in contrast to the experiments reported here, iontophoretic EPSLPs were produced mostly at spatially separated dendritic sites.

NMDA spikes could contribute uniquely to synaptic processing. First, NMDA spikes are localized to the input dendrite, potentially allowing a degree of parallel processing and independent decision making in different basal branches. This is in contrast to the local calcium spikes in the apical tufts of layer 5 neurons, which propagate for several hundred micrometres within the apical dendritic tree[4]. Second, initiation of basal dendritic spikes may be modulated by previous synaptic activity. Pre-bound glutamate on NMDA receptors will, in effect, temporarily turn them into purely voltage-gated channels, and will prime basal dendrites for initiation of NMDA spikes. We speculate that this in turn could allow the cortical circuitry to generate 'dynamic decision zones' on the dendrites of a given neuron. In principle, changes in the ensemble firing pattern of the local neural network could lead to changes in the distribution of primed NMDA conductance 'hot spots' on its constituent neurons. Third, NMDA spikes may provide an efficient mechanism for NMDA-dependent long-term synaptic strengthening[5] of co-activated neighbouring synapses without the participation of back-propagating action potentials. □

## Methods

### Slice preparation and electrophysiological recordings

Brain slices 300–350 μm thick were prepared from sensory–motor areas of 12–35-day-old rat brains as previously described[6]. We carried out whole-cell patch-clamp recordings from visually identified layer 5 pyramidal neurons[7]. The extracellular solution contained (in mM) 125 NaCl, 25 $NaHCO_3$, 25 glucose, 3 KCl, 1.25 $NaH_2PO_4$, 2 $CaCl_2$, 1 $MgCl_2$, pH 7.4. The intracellular solution contained (in mM) 115 $K^+$-gluconate, 20 KCl, 2 Mg-ATP, 2 $Na_2$-ATP, 10 $Na_2$-phosphocreatine, 0.3 GTP, 10 HEPES, 0.15-0.5 Calcium Green-1 (CG1) or 0.2 Oregon Green 488 Bapta-1 (OGB-1), pH 7.2. The electrophysiological recordings were performed using an EPC-7 (List-Electronics), and the data were acquired and analysed using PClamp 6.0 (Axon Instruments), Pulse (Heka Elektronik) and Igor (Wavemetrics) software. Focal synaptic stimulation[8] was performed through a theta patch pipette located close to the selected basal dendritic segment, guided by the fluorescent image of the dendrite. In these experiments the neurons were filled with 200 μM OGB-1 (Molecular Probes) and the basal dendritic tree was imaged with a confocal imaging system equipped with a two-photon laser (see imaging procedures). In some experiments the calcium channel blocker D-890 (B44280, 2mM, Knoll AG) was added to the recording pipette. Uncaging and synaptic experiments were performed at room temperature and at 36 °C, respectively. The size of the stimulated basal dendritic segment was assessed using calcium imaging and was found to be 10–20 μm.

### Uncaging and imaging procedures

Caged glutamate (γ-ANB-caged L-glutamic acid, Molecular Probes) was photolysed by a 361-nm ultraviolet-laser beam (Innova 300, Coherent) using 1-ms shuttered pulses (UniBlitz shutter driver/timer). After establishing a stable whole-cell recording, we perfused the recording chamber with extracellular solution (bubbled with 95% $O_2$/5% $CO_2$) containing freshly prepared caged glutamate compound (1 mM). The basal dendritic arborization was visualized (see imaging techniques for details), the ultraviolet laser was directed to the dendritic region of choice, and brief ultraviolet laser pulses (1 ms) were administered to evoke EPSLPs. The full width at half-maximum size of the


© 2000 Macmillan Magazines Ltd

photolysed spot was 6.5 ± 3 μm in brain slices, as measured by caged fluorescein dextran (Fig. 1a, dextran BMNB-caged fluorescein, Molecular Probes). Moving the laser excitation horizontally or vertically so that the basal dendrite was more than 15–20 μm from the centre of laser excitation eliminated the EPSLP altogether ($n = 5$). Excitatory postsynaptic-like potentials evoked by glutamate uncaging at a rate of 1–2 $min^{-1}$ remained stable over the time period tested (up to 40 min, $n = 9$). Blocking both AMPA and NMDA receptors with CNQX (10 μM) and AP5 (50–150 μM) eliminated the response during glutamate uncaging ($n = 4$).

### Imaging techniques

Neurons were loaded with either CG1 (150–500 μM) or OGB-1 (200 μM) through the recording patch pipette and the basal dendritic tree including dendritic spines was imaged. For calcium imaging we used two experimental setups. Experiments using focal glutamate uncaging were performed on an MRC 600 confocal scan head (Bio-Rad) equipped with both an argon ion 488-nm laser (Ion Laser Technology) and a 880-nm two-photon laser (Innova 400 pumping a Mira 900, Coherent) mounted on an upright BX50WI Olympus microscope equipped with a 60× (Olympus 0.9 NA) water objective. Full images were obtained with a temporal resolution of 1 Hz and analysed using Analyse software (Mayo Foundation). Experiments using focal synaptic stimulation were performed using a modified confocal scan head (TCS 4D, Leika Microsystems) mounted on an upright BX50WI Olympus microscope equipped with a 40× (LUMPlanFl 40XW0.9IR, Olympus) water immersion objective. Data were obtained in the line scan mode with a temporal resolution of 4.5 ms and analysed with Igor software[8].

### Modelling procedure

Computer simulations were performed using the compartmental modelling package NEURON[9] on a Pentium II PC under Windows NT. The modelling was performed on a reconstructed thick tufted layer 5 pyramidal cell. The neuron was reconstructed by A. Larkman as described[10]. The cell had 49 basal and 48 apical segments (branches) and a soma diameter of 18.5 μm. All the results shown are from inputs halfway along the first terminal basal segment. This had a length of 258 μm and a diameter of 0.84 μm after correction for shrinkage and after the spine collapse procedure. The integration method was CNEXP (Crank-Nicholson Exponential) with a time step of 25 μs. The temperature (Celsius parameter) was 25 °C. Passive parameters were modified from ref. 10 to match the decay time constants and amplitudes of modelled and experimental basal dendritic spikes.

In the model we used fast sodium, intermediate speed low voltage-activated, T-type (CaT) calcium, high voltage-activated calcium (CaH), NMDA and AMPA conductances. A modified Hodgkin–Huxley scheme was used for voltage-sensitive conductances, and the parameters for the voltage gated and synaptic conductances were based on published experimental data[11–17]. Some of the parameters were modified to allow better fit of the experimental results, and selected model parameters, including conductances (or densities), were varied manually to achieve a good match between the model and the experimental results. NEURON files can be obtained from G.M. (e-mail: gm@physiol.ox.ac.uk).

Received 2 November 1999; accepted 5 January 2000.


1. Larkman, A. U. Dendritic morphology of pyramidal neurons of the rat: Spine distribution. *J. Comp. Neurol.* **306,** 332–343 (1991).
2. Cash, S. & Yuste, R. Input summation by cultured pyramidal neurons is linear and position independent. *J. Neurosci.* **18,** 10–15 (1998).
3. Cash, S. & Yuste, R. Linear summation of excitatory inputs by CA1 pyramidal neurons. *Neuron* **22,** 383–94 (1999).
4. Schiller, J., Schiller, Y., Stuart, G. & Sakmann, B. Calcium action potentials in apical dendrites of neocortical pyramidal neurons in rat brain slices. *J. Physiol.* **505,** 605–616 (1997).
5. Bliss, T. V. P. & Collingridge, G. L. A synaptic model of memory: Long term potentiation in the hippocampus. *Nature* **361,** 31–39 (1993).
6. Schiller, J., Schiller, Y. & Clapham, D. E. NMDA receptors amplify calcium influx into dendritic spines during associative pre- and postsynaptic activation. *Nature Neurosci.* **1,** 114–118 (1998).
7. Stuart, G. J., Dodt, H. U. & Sakmann, B. Patch-clamp recordings from the soma and dendrites of neurons in brain slices using infrared video microscopy. *Pflug. Arch. Eur. J. Physiol.* **423,** 511–518 (1993).
8. Koester, H. J. & Sakmann, B. Calcium dynamics in single spines during coincident pre- and postsynaptic activity depend on relative timing of back-propagating action potentials and subthreshold excitatory postsynaptic potentials. *Proc. Natl Acad. Sci. USA* **95,** 9596–9601 (1998).
9. Hines, M. L. & Carnevale, N. T. The NEURON simulation environment. *Neural Comput.* **9,** 1179–1209 (1997).
10. Major, G., Larkman, A. U., Jonas, P., Sakmann, B. & Jack, J. J. B. Detailed passive cable models of whole-cell recorded CA3 pyramidal neurons in rat hippocampal slices. *J. Neurosci.* **14,** 4613–4638 (1994).
11. Ascher, P. & Nowak, L. The role of divalent cations in the *N*-methyl-D-aspartate responses of mouse central neurons in culture. *J. Physiol.* **399,** 247–266 (1988).
12. Hestrin, S., Nicoll, R. A., Perkel, D. J. & Sah, P. Analysis of excitatory synaptic action in pyramidal cells using whole-cell recording from rat hippocampal slices. *J. Physiol.* **422,** 203–225 (1990).
13. Brodin, L., Traven, H. G. C., Lansner, A., Wallen, P. & Ekeberg, O. Computer simulations of *N*-methyl-D-aspartate receptor-induced membrane properties in a neuron model. *J. Neurophysiol.* **66,** 473–484 (1991).
14. Brown, A. M., Schwindt, P. C. & Crill, W. E. Voltage dependence and activation kinetics of pharmacologically defined components of the high-threshold calcium current in rat neocortical neurons. *J. Neurophysiol.* **70,** 1530–1543 (1993).
15. Jonas, P., Major, G. & Sakmann, B. Quantal components of unitary EPSCs at the mossy fiber synapse on CA3 pyramidal cells of rat hippocampus. *J. Physiol.* **472,** 615–663 (1993).
16. Martina, M. & Jonas, P. Functional differences in $Na^+$ channel gating between fast-spiking interneurons and principal neurons of rat hippocampus. *J. Physiol.* **505,** 593–603 (1997).
17. Destexhe, A., Neubig, M., Ulrich, D. & Huguenard, J. Dendritic low-threshold calcium currents in thalamic relay cells. *J. Neurosci.* **18,** 3574–3588 (1998).



### Acknowledgements

We thank. D. E. Clapham, F. Prendergast, B. Sakmann, W. Denk and D. Tank for assistance and support, A. Larkman for reconstructing the cell used in the simulations, and M. Hausser and G. Stuart for reading early versions of the manuscript. In addition we thank the Mayo Foundation, Leo & Frances Kogan endowment fund (J.S.), Wellcome Trust, Lucent Technologies and Marine Biological Laboratory (G.M.) for financial support.


Correspondence and requests for materials should be addressed to J.S. (e-mail: Jackie@tx.technion.ac.il).

# The Ras-MAPK pathway is important for olfaction in *Caenorhabditis elegans*

**Takaaki Hirotsu, Satoshi Saeki*†, Masayuki Yamamoto* & Yuichi Iino**

*Molecular Genetics Research Laboratory, The University of Tokyo, Tokyo 113-0033, Japan*
** Department of Biophysics and Biochemistry, Graduate School of Science, The University of Tokyo, Tokyo 113-0033, Japan*

**The Ras-MAPK (mitogen-activated protein kinase) signal transduction pathway is well known to control cellular proliferation and differentiation in response to extracellular signals, but its other functions are less understood. In *Caenorhabditis elegans* this pathway regulates several developmental events, such as vulval induction and progression of meiosis[1], but its function in the nervous system is unknown. Here we report that the Ras-MAPK pathway is involved in olfaction in this organism. Mutational inactivation and hyperactivation of this pathway impairs efficiency of chemotaxis to a set of odorants. Experiments in which *let-60 ras* was expressed using a heat-shock promoter and a cell-specific promoter show that a normal activity of LET-60 Ras is required in mature olfactory neurons. Application of the odorant isoamylalcohol to wild-type animals leads to the activation of MAP kinase in olfactory neurons within 10 seconds. This induction is dependent on the function of the nucleotide-gated channel TAX-2/TAX-4 and the voltage-activated calcium channel subunit UNC-2. These results suggest a dynamic regulatory role for the Ras-MAPK pathway in perception and transmission of sensory signals in olfactory neurons.**

Chemotaxis to volatile chemoattractants in *C. elegans* is mediated primarily by two pairs of olfactory neurons, AWA and AWC (ref. 2). The gain-of-function (gf) mutant of *let-60 ras*, *let-60(n1046*gf*)*, shows a defect in chemotaxis to the AWC-sensed chemoattractants isomylalcohol (Fig. 1a, open bars), butanone and benzaldehyde (data not shown). It also shows a weak but statistically significant defect in chemotaxis to the AWA-sensed chemoattractant diacetyl (Fig. 1b, open bars). This oncogenic-type mutation in *let-60* is expected to lead to a reduced rate of conversion from the GTP-bound active form to the GDP-bound inactive form, and therefore hyperactivation, of the encoded Ras protein[3]. Defects in chemotaxis to AWA- and AWC-sensed odorants are also seen in the loss-of-function (lf) mutants *let-60(n2021)* and *lin-45(sy96)* and the

† Present address: Tokyo Research Laboratories, Kyowa Hakko Kogyo Co., Ltd, Machidashi, Tokyo 194-8533, Japan.


© 2000 Macmillan Magazines Ltd